Improved moving particle semi-implicit method with adaptive variable-size particles

***Kai Zhang, †Zhongguo Sun, Xiao Chen, Qixin Liu, and Guang Xi**

School of Energy and Power Engineering, Xi'an Jiaotong University, China

*Presenting author: zk2017@stu.xjtu.edu.cn

†Corresponding author: sun.zg@xjtu.edu.cn

Abstract

In order to conduct simulations with high accuracy using particle methods, numerous particles with small size are required to increase the resolution of the calculation domain, and furthermore an improved MPS method with variable-size VSP-MPS has been proposed to achieve the object in acceptable time. In this paper, the scheme is improved with adaptive variable-size particle as AVSP-MPS to increase computational efficiency. First, we made linear programming for the selection and changed the decision method of particle entering the different resolution to improve the robustness at coarse/fine interface, as a result, the accuracy of calculation was improved. As the high resolution of the previous multi-resolution MPS method is static, we get a moving high resolution region and proved that the region movement has no adverse effect on the flow field. At last, the scheme with adaptive variable-size particle as AVSP-MPS is introduced, the shape and area of the domains with high resolution can be dynamically adjusted during the calculation. The proposed method was verified by simulating dam-break case with a moving obstacle. The computing time for the cases with and without AVSP-MPS was analyzed to prove its capability on reducing the computational cost.

Keywords: adaptive variable-size particles, coalescence, split, moving multi-resolution region, computational efficiency

1 Introduction

In classical grid-based computational methods, variable resolution can be easily achieved though refined structured/unstructured grids to improve accuracy in specific computational domains. Particle-based methods such as moving particle semi-implicit (MPS)[1] method is widely used for analyzing unsteady flow with large deformation, however, with the increase of calculation accuracy and scale, it takes large amount of particles to adopt a single resolution, and the calculation is time-consuming. To reduce the computational cost, several methods have been developed in smoothed particle hydrodynamics (SPH)[2] and MPS simulations.

Different with incompressible flow simulation in MPS, SPH is generally used to solve compressible flow, the incompressible flow is usually solved by introducing a weakly compressible scheme (WCSPH). In order to reduce computer time, Omidvar[3] produced a variable particle mass distribution with fine resolution near the body and coarse resolution further away. Though two well-defined test cases of waves generated by a heaving semi-immersed cylinder and progressive waves interacting with a fixed cylinder, the variable mass distribution leads to a computer run speedup of nearly 200%. Feldman[4] proposed a dynamic particle refinement method where candidate particles are split into several 'daughter' particles according to a given refinement pattern. In such a method, the daughter particle properties

such as mass, volume, density, velocity and pressure are chosen so that both energy and mass are conserved. Vacondio[5] modified dynamically the particle sizes by means of splitting and coalescing (merging) individual particles, their simulations have shown that the particle refinement procedure is able to increase the efficiency while maintaining the same level of accuracy as a uniform distribution with the most refined resolution. Chiron[6] presented the basics of an Adaptive Particle Refinement (APR) technique, inspired by Adaptive Mesh Refinement (AMR)in mesh-based methods. This approach ensures robustness at coarse/fine interfaces with alleviated constraints. Sun[7-8] implemented a particle shifting technique (PST) in the framework of δ^+-SPH combining with APR which is a numerical technique adopted to refine the particle resolution in the local region and de-refine particles outside that region. The problems of high computational costs and tensile numerical instability are avoided in δ^+-SPH scheme since APR and Tensile Instability Control (TIC) have been implemented.

Most of the above attempts based on SPH were implemented with the explicit algorithm to produce the pressure field. However, a semi-implicit algorithm is often adopted to obtain the pressure field in MPS method, which need to solve the pressure Poisson equation and makes it much more difficult developing the local refine technique in the MPS than that in the SPH. Shibata[9-10] developed a multi-resolution technique, the overlapping particle technique (OPT), the OPT expresses a whole simulation domain with partially overlapping sub-domains with their own spatial resolutions and particle shape. Despite the improvements, because the mass or volume conservation of the particle size conversion procedure is not thoroughly discussed in OPT, the total mass conservation of the algorithm needs to be studied and guaranteed. Tanaka[11] developed further a multi-resolution technique for the MPS method in two dimensions, however, the formulation was derived for the classical MPS method and thus it suffers from inaccuracy and stability issues. Tang[12] extended this method for three dimensions, however, no splitting or merging algorithms were adopted and therefore the spatial resolution cannot be changed dynamically. Chen[13] developed a multi-resolution MPS method with variable-size particles based on an algorithm for dynamic particle coalescing and splitting. For the existing surface detection technique could not avoid misdetection, the dynamic particle refinement is also incorporated based on an improved MPS method with no surface detection (NSD-MPS)[14]. Besides, a new gradient model associated with different particles sizes is used and all effective radii of particles remain the same ensures the conservation of mass and momentum in VSP-MPS method. Tanaka[15] developed novel boundary conditions for the treatment of wall and pressure boundaries for the multi-resolution least square MPS method, the new boundary condition makes the method easier to be used in flow simulations of channel flows.

However, for all of the above MPS methods, the domains with different sized particles are set before calculation and their location/area are fixed, which makes it cumbersome when simulating the fluid flow cases with a moving object. In this paper, we improved the moving particle semi-implicit method with adaptive variable-size particles as AVSP-MPS. The spatial resolution varies dynamically with the location of the interface between liquid and the moving objects, the different resolution areas don't need to be known beforehand. In order to optimize the splitting and coalescing algorithm, we made linear programming for the selection of resolution and got the optimal resolution interval. In addition, we changed the decision method of particle entering the different resolution to improve the robustness at coarse/fine interfaces. Based on the above improvements, the dam-break case with a moving object was simulated with different methods. Compared with the VSP-MPS method which can only delimit the resolution region in advance, with an adaptive algorithm, AVSP-MPS method can

further reduce the number of particles needed in the simulation and improve the calculation efficiency.

2 VSP-MPS Methods

This section recalls the MPS method with variable-size particles, the governing equations for an incompressible flow are:

$$\frac{D\rho}{Dt} + \rho\nabla \cdot \mathbf{u} = 0 \tag{1}$$

$$\rho\frac{D\mathbf{u}}{Dt} = -\nabla p + \mu\nabla^2\mathbf{u} + \mathbf{f} \tag{2}$$

where **u** represents velocity vector, t is time, ρ is the constant density, p is pressure, μ is dynamic viscosity and **f** is the volumetric force, such as gravity.

2.1 Kernel Function

The cubic spline kernel function, which is usually used in SPH, was used in this paper:

$$w_{ij}(R_{ij}) = \alpha \times \begin{cases} 2/3 - R^2 + 0.5R^3 & (R \le 1) \\ 1/6 * (2-R)^3 & (1 < R \le 2) \\ 0 & (R > 2) \end{cases} \tag{3}$$

$$R = r / h \tag{4}$$

$$\alpha = 15/(7\pi h^2) \tag{5}$$

where r is the distance between neighboring particles, $h = 2.1l_0$ is used for all particles in this paper, l_0 is the initial particle size, and α is the normalization coefficient. With the kernel function, the particle number density can be calculated as:

$$n = \sum w_{ij} V_j \tag{6}$$

where w_{ij} is the kernel function between particle i and j, and V_j is the volume of particle j. The constant particle number density is $n^0 = 1.0$ for standard particle distribution.

Figure 1 shows three possible cases between two adjacent particles. For example, particle i may overlap with particle j as shown in Figure 2(a), in this case, the density attribution of j to i is $w_{ij}V_j$ using Eq. (3), while the density of i is $\rho(V_i + V_j)/\max(V_i, V_j)$. In order to avoid particle clustering, an additional weight function[13] is introduced:

$$w_{a,ij} = \begin{cases} 0 & (R_{a,ij} > 1) \\ (1 - 1.5R_{a,ij}^2 + 0.5R_{a,ij}^3)^2 / V_{\max} & (1 \ge R_{a,ij} \ge 0) \\ 1/V_{\max} & (R_{a,ij} < 0) \end{cases} \tag{7}$$

$$R_{a,ij} = \frac{r_{ij} - 0.5\left|l_j - l_i\right|}{0.5(l_j + l_i - \left|l_j - l_i\right|)} \tag{8}$$

where the subscript a represents the additional function, $V_{\max} = \max(V_i, V_j)$ is the maximum volume between the two particles (where $V_i = l_i^2$ and $V_j = l_j^2$), l_i and l_j are the diameters of particle i and j respectively.

When $r_{ij} \geq 0.5(l_i + l_j)$ (Figure 2(c)), the additional weight function $w_{a,ij}$ is zero. When $r_{ij} < 0.5\left|l_j - l_i\right|$ (Figure 2(a)), the density attribution of j to i is $V_j / V_{\max}$, $w_{a,ij} = 1/V_{\max}$. When $0.5\left|l_j - l_i\right| \leq r_{ij} \leq 0.5(l_i + l_j)$ (Figure 2(b)), a monotone decreasing function $(1-1.5R_{a,ij}^2 + 0.5R_{a,ij}^3)^2$ is used to represent the value of $w_{a,ij}$ from $1/V_{\max}$ to zero.

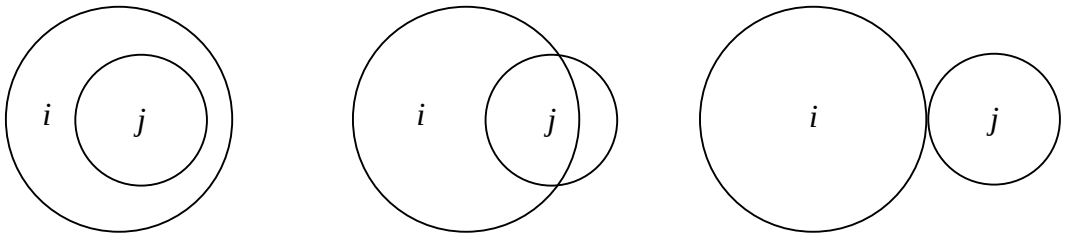

(a) overlapping particles (b) clustering particles (c) adjacent particles

Figure 1. Position relationships between two particles

2.2 Particle Interaction Models

A new gradient model is used in this paper to ensure the conservation of momentum[16].

$$\left\langle \nabla \phi \right\rangle_i = \frac{d}{\lambda_1 n^0} \sum_{j \neq i} \left[\frac{\phi_j + \phi_i}{\left| r_{ij} \right|} \vec{r}_{ij} w_{ij} \right] \tag{9}$$

The parameters λ_1 is defined as

$$\lambda_1 = \frac{\int_v w(r) r dv}{\int_v w(r) dv} \tag{10}$$

The gradient (9) is totally irrelevant from particles' distance, and the influence from the particles with different sizes could be ignored.

The original Laplace model introduced by Koshizuka[1] is used in this paper

$$\left\langle \nabla^2 \phi \right\rangle_i = \frac{2d}{n^0 \lambda_2} \sum_{j \neq i} \left[\left(\phi_j - \phi_i \right) w_{ij} \right] \tag{11}$$

The parameters λ_2 is defined as

$$\lambda_2 = \frac{\int_v w(r) r^2 dv}{\int_v w(r) dv} \tag{12}$$

The pressure Poisson equation introduced by Tanaka[16] is used in this paper:

$$\nabla^2 P_i = (1-\gamma) \frac{\rho}{\Delta t} \nabla \cdot \vec{u}_i^* + \gamma \frac{\rho}{\Delta t^2} \frac{n^0 - n_i^n}{n^0} \tag{13}$$

where n_i^n is the particle number density in the n^{th} steps and $\gamma = 0.008$ is a coefficient.

2.3 Free Surface boundary Conditions

The original MPS method may misjudge surface particles when the solving the pressure Poisson equation with multi-resolution, which has an adverse effect on the accuracy of calculation. Thus, a new algorithm of MPS method with no surface detection (NSD-MPS)[14] can improve computational stability by avoiding surface particle detection. The NSD-MPS method ensures that all real particles have the particle number density more than n^0 in the whole region by introducing conceptual particles to compensate for the loss of particle number density. The Dirichlet boundary condition of the pressure Poisson equation is enforced by the conceptual particles, which have the free surface pressure P_{free}, that is to say, the conventional surface particles are replaced by conceptual particles to take the zero-pressure condition. You can get more details in reference [14].

2.4 Particle Splitting and Coalescing Methodology

In order to increase the resolution in certain areas of the computational domain, particle splitting and coalescing were involved in the algorithms. In previous methods, the momentum tends to be non-conservation, especially in the process of fine resolution to coarse resolution, particles need to wait or be deleted in the simulation. In VSP-MPS method, we cancel the restriction, different particle sizes are allowed in the region, which can achieve momentum conservation. At the same time, different resolutions are determined by a maximum volume $V_{\max}$ and a minimum volume $V_{\min}$. A particle that is larger than $V_{\max}$ would be split into seven daughter particles, while a particle that is smaller than $V_{\min}$ would be coalesced with a neighboring particle. With several processes of splitting and coalescing, the size of particles in the region is limited to a certain range, which is conducive to controlling the number of particles and improving the computational efficiency.

2.4.1 Particle splitting

In particle splitting processes[13], a mother MPS particle splits into 7 daughter particles, and the volumes of the daughter particles are equal to 1/7 of mother particle. In order to meet the Newton's third law, all particles including the new daughter particles share the same smoothing length $h = 2.1l_0$.

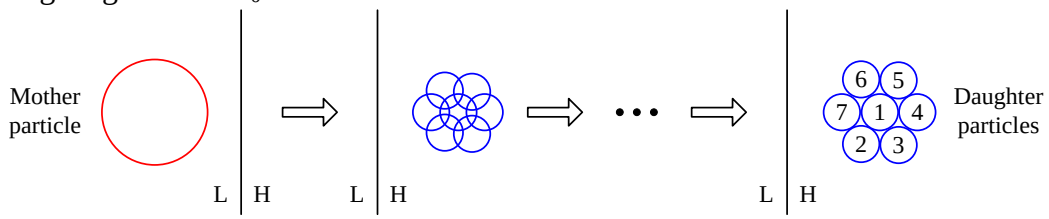

(*a*) splitting process

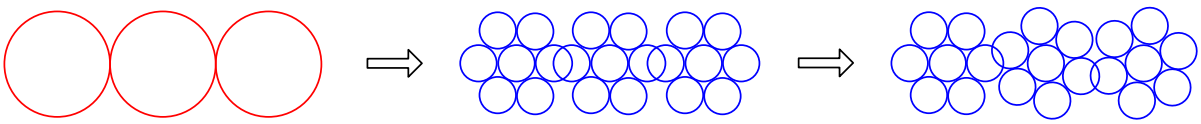

(*b*) random splitting angles to avoid particle clustering

Figure 2. Large particles splitting into daughter particles

where the solid straight line represents the demarcation line of different resolutions. Here, the left side of the demarcation line is the low resolution area, as expressed with L at the left side, and the right side is the high resolution area, as expressed with H at the right side.

Figure 2(*a*) is the sketch of a process of a particle splitting into seven daughter particles. The daughter particle 1 locates at the same position as the mother particle, and the other six

daughter particles are distributed to form a regular hexagon around particle 1. Daughter particles are distributed with a small overlap in the first splitting process to decrease particle clustering, then the daughter particles move away from other particles with a small distance in the rest steps so that the CFL condition of MPS is met, the splitting process will be finished in five steps. Furthermore, an algorithm will be used to lead the daughter particles to form a random angle as shown in Figure 2(*b*), and to guide the particles moving to proper positions. The algorithm would further reduce the possibility of particle clustering. The velocity vectors of the daughter particles are set equal to that of their mother particle for linear momentum conservation in the five steps during the splitting process. The daughter particles would have no angular velocity at the first step of splitting because the mother particle has no angular momentum.

2.4.2 Particle coalescing

Particle coalescing process[13] will conduct between two neighboring particles as shown in Figure 3, fine particles will coalesce with other particles if their volume is smaller than given minimum volume $V_{\min}$. Similar to the splitting process described previously, a five-step coalescing process will be used to avoid particle clustering, and the additional weight function (Eq. (6)) won't be used between the two particles during coalescing process.

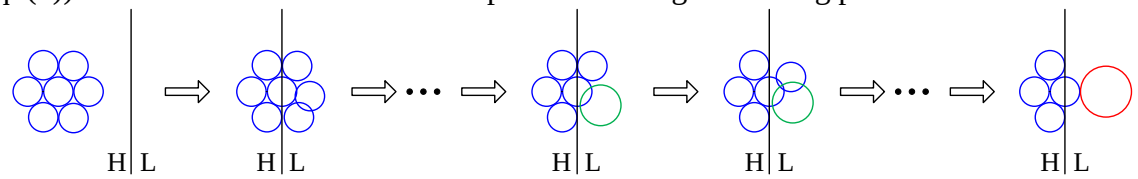

Two particle coalescing processes with ten steps

Figure 3. Sketch of particle coalescing processes

Considering the incompressibility and mass conservation, the volume of the new particle (new particle is represented by M) V_M is calculated as:

$$V_M = V_i + V_j \tag{14}$$

For momentum conservation, during coalescing, the position and velocity vector of mass center are:

$$\vec{r}_M = \frac{V_i \vec{r}_i + V_j \vec{r}_j}{V_M} \tag{15}$$

$$\vec{v}_M = \frac{V_i \vec{v}_i + V_j \vec{v}_j}{V_M} \tag{16}$$

And for angular momentum, the coalescing two particles would have velocities

$$\vec{\theta}_M = \frac{\left(\vec{r}_i - \vec{r}_M\right) \times \left(\vec{v}_i - \vec{v}_M\right) \cdot V_i + \left(\vec{r}_j - \vec{r}_M\right) \times \left(\vec{v}_j - \vec{v}_M\right) \cdot V_j}{\left|\vec{r}_i - \vec{r}_M\right|^2 \cdot V_i + \left|\vec{r}_j - \vec{r}_M\right|^2 \cdot V_j} \tag{17}$$

$$\vec{v}_i = \vec{v}_M + \left(\vec{r}_i - \vec{r}_M\right) \times \vec{\theta}_M \tag{18}$$

$$\vec{v}_j = \vec{v}_M + \left(\vec{r}_j - \vec{r}_M\right) \times \vec{\theta}_M \tag{19}$$

where $\vec{\theta}_M$ is the angular velocity. After the coalescing, the two particles merged into one large particle without angular velocity.

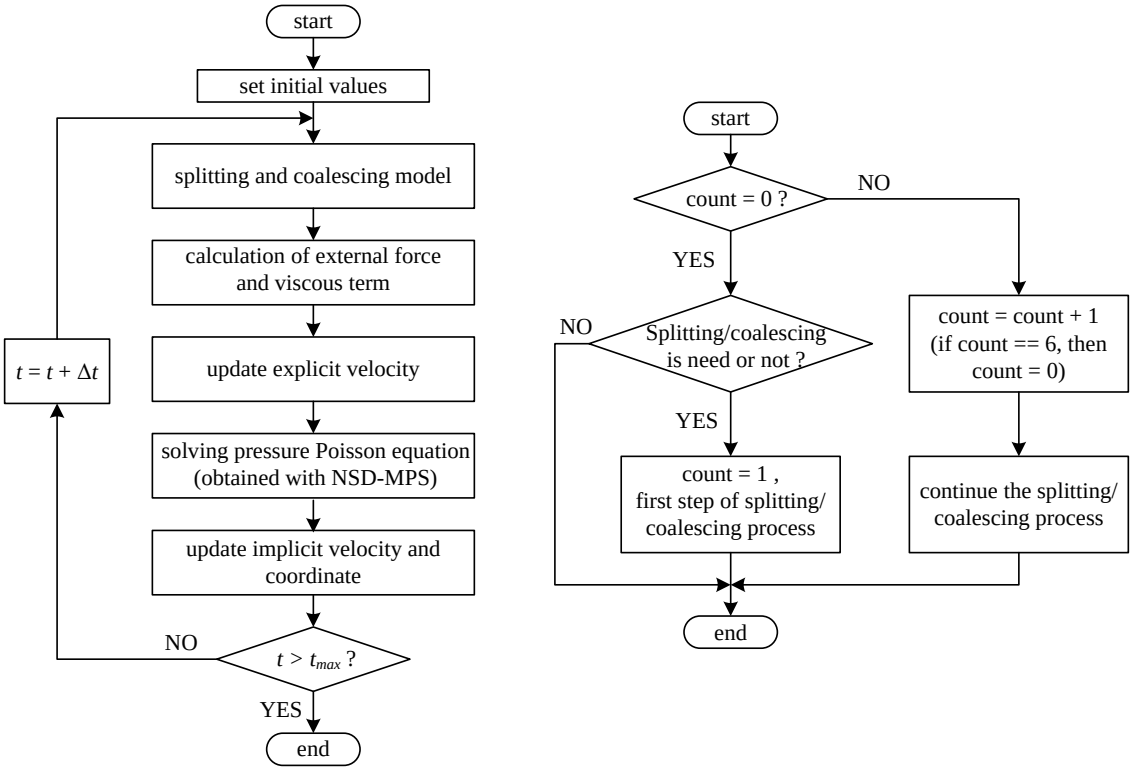

(*a*) VSP-MPS (*b*) the splitting/coalescing model

Figure 4. Flowcharts of the VSP-MPS method and the splitting/coalescing model

Figure 4(a) shows the flowchart of the VSP-MPS method, and Figure 4(b) shows the flowchart of the splitting/coalescing model. The number count represents the status of the splitting/coalescing model, count = 0 means no the splitting/coalescing model, and count=1-5 represents the step of the splitting/coalescing process from 1 to 5. To save computational cost, splitting and coalescing processes share a same five-step process, in other words, the splitting and coalescing processes are initiated every five steps by checking their criteria respectively, there is no new splitting and coalescing process during the five steps.

3 Numerical Verification

A Dam-break case is simulated to verify the VSP-MPS method along with the particle splitting and coalescing schemes in this section. The case is simulated with single resolution and variable resolution respectively to verify the accuracy of the VSP-MPS method and its effectiveness on improving the computational efficiency.

The initial setup of the dam-break case is shown in Figure 5. $V_{\max}$ and $V_{\min}$ are the maximum and minimum volumes to control the particle splitting and coalescing processes in our algorithm. The physical parameters of fluid particle used in this case are $\rho = 988\text{kg/m}^3$ and $\nu = 1.0 \times 10^6\text{m}^2/\text{s}$. In the single resolution case, the initial diameter of water particles is $l_0 = 0.0019\text{m}$, the particle is 5672, in which 3200 are fluid particles. In the variable resolution case, the initial diameter of water particles is $l_0 = 0.005\text{m}$, the fluid particle will split or coalesce during the simulation, and the diameter of the particles will be 0.0019m after once splitting process.

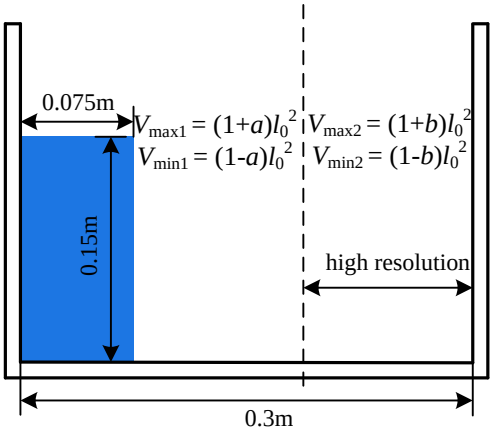

Figure 5. Geometry of the dam-break case

3.1 Repartition of the Resolution

The resolution is realized by setting the maximum and minimum volume of particles in different regions. In order to improve efficiency, we made linear programming for the selection of resolution and got the optimal resolution interval.

The upper and lower bounds of the intervals in different resolution regions are shown in Figure 5. Although the errors caused by the inconsistency of particle sizes can be mitigated by using the kernel function and the interaction model given in section 2. If the difference between V_{min} and V_{max} is too large in the same resolution region, all the particles meet this region would stay and coalesced would not happen, the number of the particles was large and the calculation efficient was low. On the other hand,, if the difference between V_{min} and V_{max} is too small, the split and coalesce process may happen and repeat until the size of the particle meet the narrow interval. The calculation efficient was also low by carrying out more split/coalesce process.

In order to reduce the number of splitting and coalescing process, after the splitting of the smallest particle and the largest particle, the split particles will not split and coalesce again in the low resolution region.

$$1-a \le \frac{1/7+b+1+a}{7} \le 1+a \tag{20}$$

$$1-a \le \frac{1+a}{7} \le 1+a \tag{21}$$

In high resolution regions, the largest and smallest particles that need to be split do not split and coalesce after once splitting.

$$\frac{1}{7}-b \le \frac{1+a}{7} \le \frac{1}{7}+b \tag{22}$$

$$\frac{1}{7}-b \le \frac{(1+b)/7}{7} \le \frac{1}{7}+b \tag{23}$$

At the same time, in order to maintain the continuity of particle diameter, the V_{min} of low resolution region should be smaller than the V_{max} of high resolution region.

$$1-a \le \frac{1}{7}+b \tag{24}$$

It is certain that V_{min1} and V_{min2} should be greater than zero to ensure the non-negativity of particle volume.

$$1-a\geq 0 \tag{25}$$

$$\frac{1}{7}-b\geq 0 \tag{26}$$

Simultaneous equation (20) - (26) gives the feasibility interval as shown in Figure 6. In order to reduce the difference of particle diameter in the same resolution region, in low resolution region, the particle diameter should be close to $V_0=l_0^2$, and the particle diameter should be close to $V_0/7=l_0^2/7$ in high resolution region, On the basis of satisfying the preceding conditions(equation (20) - (26)), the values of *a* and *b* should be as small as possible. When the weights of *a* and *b* are the same, the optimal solution is a=3/4 and b=6/50(the point marked P as shown in Figure (6)), when the weights of *a* and *b* are different, the optimal solution will not change. So after the repartition of the resolution, we get $V_{max1}=1.75l_0^2$, $V_{min1}=0.25l_0^2$, $V_{max2}=0.263l_0^2$, $V_{min2}=0.0229l_0^2$.

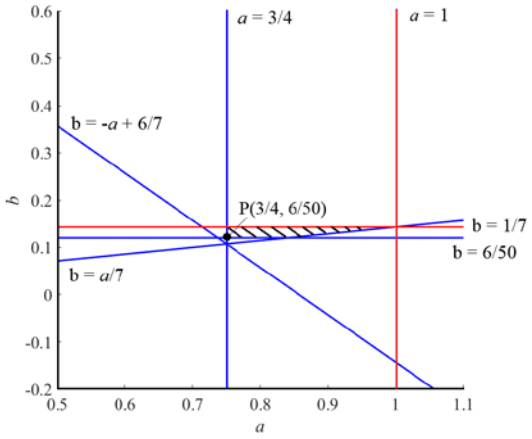

Figure 6. Optimal solution of resolution repartition

3.2 Dam-break test

Figure 7 shows the experimental and simulation results of the position of water front in the dam-break case. The horizontal axis is the non-dimensional time, $t(2g/L)^{0.5}$, and the vertical axis is the non-dimensional position of the water column's leading edge (Z/L). The VSP-MPS result with variable resolution is compared with the single resolution MPS result and the experimental results by Martin[17]. The simulation results agree with the experimental results, and compared with the single resolution MPS result, the VSP-MPS result has even higher precision in high resolution area(as shown in Fig. 7).

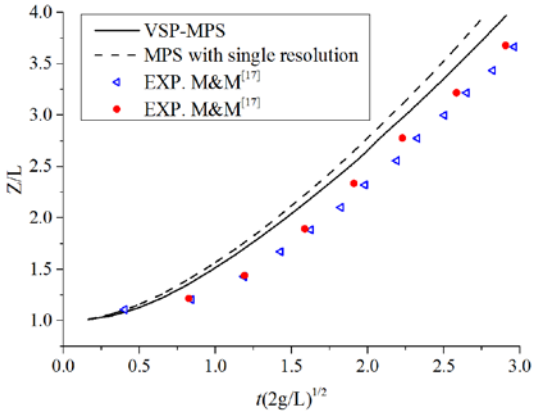

Figure 7. Experimental and simulation results of the position of water front in the dam-break problem

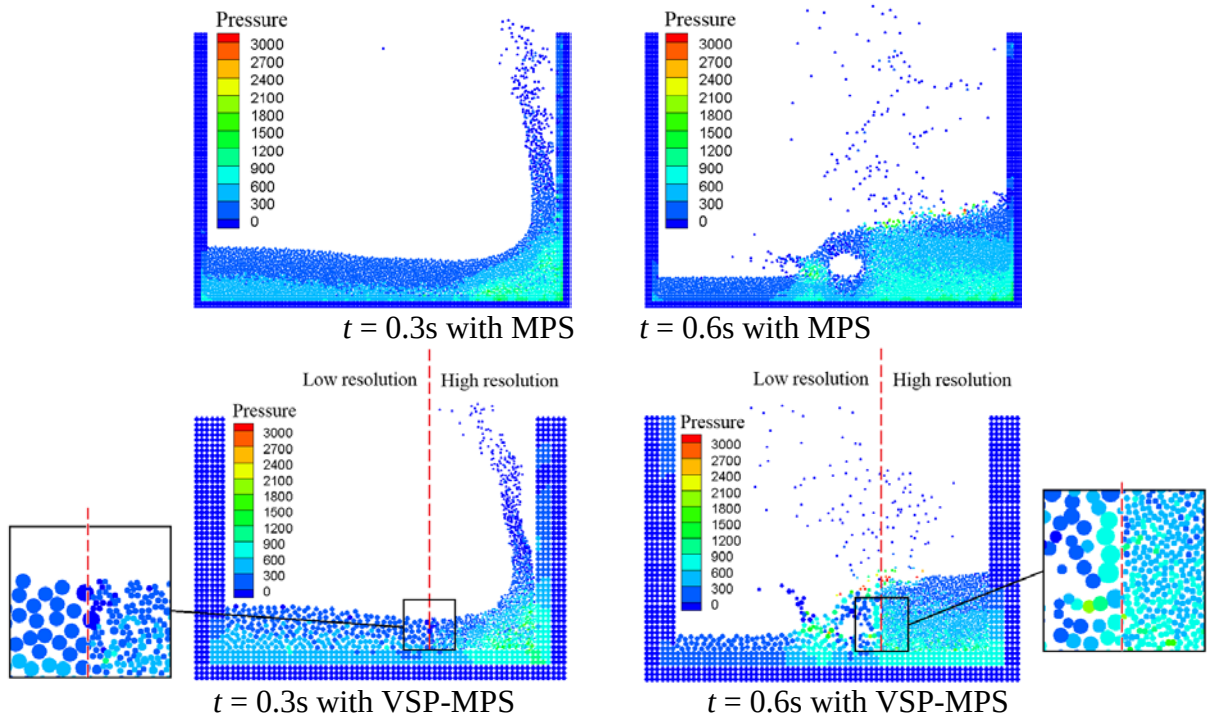

t = 0.3s with MPS *t* = 0.6s with MPS

t = 0.3s with VSP-MPS *t* = 0.6s with VSP-MPS

Figure 8. Snapshots from the dam-break simulation

Figure 8 shows the pressure distribution of fluid at two typical times with different methods, which shows that the VSP-MPS method can accurately simulate the pressure distribution of fluid in the flow process. In addition, it can be observed that coarse particles can split into fine particles after entering the high resolution region, and fine particles will coalesce with neighboring particles after entering the low resolution region. The splitting and coalescing processes are implemented until the particle volume remains within the given range. It is notable that the splitting and coalescing processes occur in the whole computational domain, instead of just at coarse/fine interface.

Figure 9 shows the comparison of particle number and CPU time with the two different methods. Compared with the single resolution MPS method, the VSP-MPS method requires fewer particles and greatly reduces the calculation time. For example, there are 5672 particles in the dam-break case with single resolution MPS, and the particle number is constant during the simulation. In VSP-MPS method, the particle number is various during the simulation, it can be divide into 5 phases during the simulation (see Figure 9(a)). There are 1422 initial setting particles at the begin of the simulation (region A), when the particle pass through the high resolution, the particle split into finer particles, so the particle number increases in this phase (region B). The particle number decrease in region C due to the fluid flow back into low resolution region and fine particle coalesces with neighboring particle. Then the fluid sloshes between the two solid walls (region D) flowing through the resolution boundary for several times before totally dissipated, At last, the fluid tends to be stable gradually(region E), and the particle number converge to be a constant.

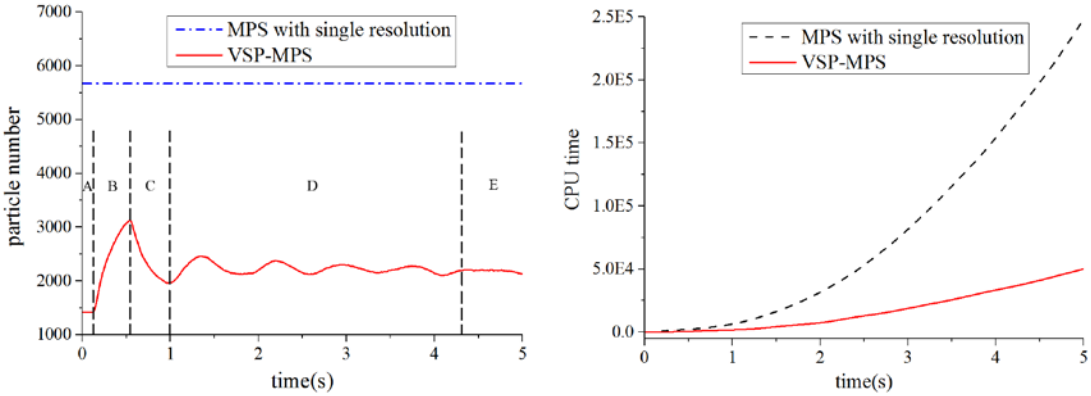

(a) Particle number (b) CPU time

Figure 9. Comparison of particle number and CPU time with different methods

As shown in Fig 9(b), the calculation time of VSP-MPS is much short than that of MPS with single resolution. Compared with single resolution MPS method, when the simulation runs to five seconds, the CPU time is reduced by 79.8% using VSP-MPS method. The above simulation results prove that the VSP-MPS method could improve the simulation accuracy and significantly raise the calculation efficiency.

4 Numerical Simulation

In VSP-MPS method, the resolution regions are mandatory to be set before the simulation, and the shapes and locations of which are fixed during the whole calculation. It is difficult for a fixed high resolution region to cover a complex flow with moving object.

In this paper, a new scheme AVSP-MPS was proposed based on VSP-MPS, the high resolution region could be adjusted during the calculation and even could tracking the location and shape of the target flow. It is much more flexible for complex flows, and the accuracy and efficiency would both be improved.

4.1 Improvement of the Algorithm Accuracy

Though the VSP-MPS method allows finer particles in specific areas and coarser particles elsewhere, the robustness on coarse/fine interface needs to be improved. In the previous algorithm, the particle will split into finer particles when the center of mass of the particle enters the high-resolution region. As a result, there will be a large number of particles of different diameters at coarse/fine interface, the numerous different diameters at coarse/fine interface will reduce the accuracy of the simulation. In order to improve the robustness at coarse/fine interface, we improved the algorithm by changing the decision method of particle entering the different resolution. The improved approach is that only when the whole particle (the boundary of the particle) enters the high resolution region the particle splitting into finer particles.

In order to validate the improved algorithm, we simulated the dynamic behavior of a single particle passing through the high resolution boundary with the unimproved algorithm and the improved algorithm. The center of the particle is initially located at coarse/fine boundary, and the particle is given a uniform rightward initial velocity u=0.1m/s. Gravity is not considered in the whole process. The comparison of particles dynamic behavior before and after improvement is shown in Figure 10.

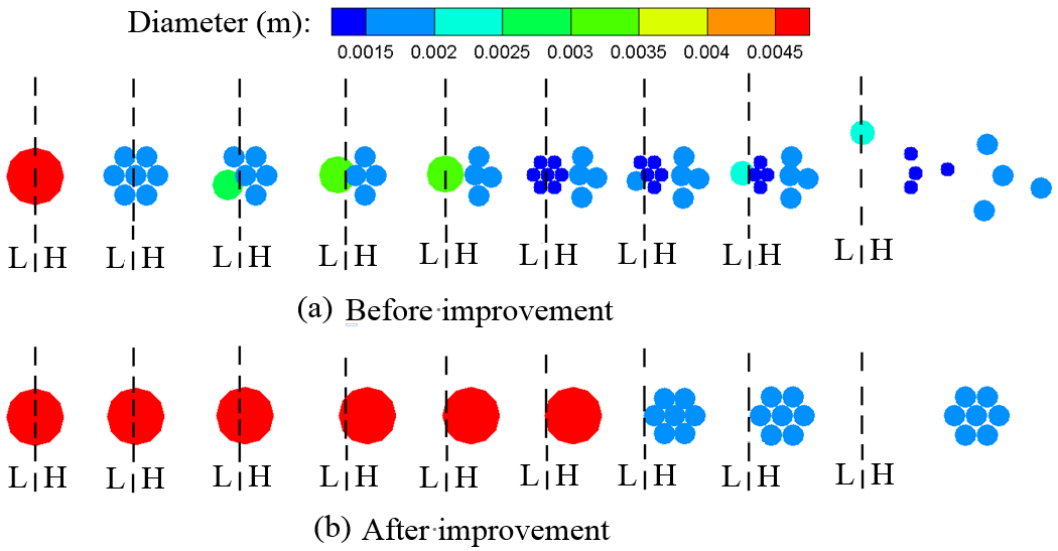

Figure 10. Comparison of particles dynamic behavior before and after improvement

where the black solid line represents the coarse/fine boundary, the left region of the boundary is low resolution, and the right region of the boundary is high resolution.

Before the improvement, the particle is divided into seven fine particles when the center of mass of the particle passes through the coarse/fine boundary. However, at this time, three fine particles stay in the low-resolution region. After two coalescing processes, one coarse particle and four fine particles are formed. Then the coarse particles will continue to split and form seven finer particles when it passes through the coarse/fine boundary. The finer particles, reside in the low resolution region, are coalesced twice, and finally nine particles with three different diameters are obtained.

After the improvement, the particle splits into 7 finer particles when the left boundary of the particle enters the high resolution region, all finer particles have a velocity of u = 0.1m/s due to momentum conservation. The particles keep moving rightward at a constant speed. On the contrary, before the improvement, the particle interaction with different velocities makes the particle motion more complex, and the velocity of particles changes after they passing through the coarse/fine boundary, it has an adverse effect on the algorithm accuracy.

After the improvement, there is no finer particle staying in low resolution region, the dynamic behavior of the particle is simpler, the number of splitting and coalescing processes decreases, and the robustness of the coarse/fine interface is improved. We further simulate the dam-break case as shown in Figure 5 with the unimproved algorithm and the improved algorithm respectively. The physical parameters of fluid particle used in this paper are ρ = 988kg/m^3 and v = 1.0 × 10^{6}m^2/s, the initial diameter of the fluid particles is l_0 = 0.005m. Figure 11 shows the comparison of particle diameter numbers before and after the improvement near coarse/fine interface and in the whole calculation area.

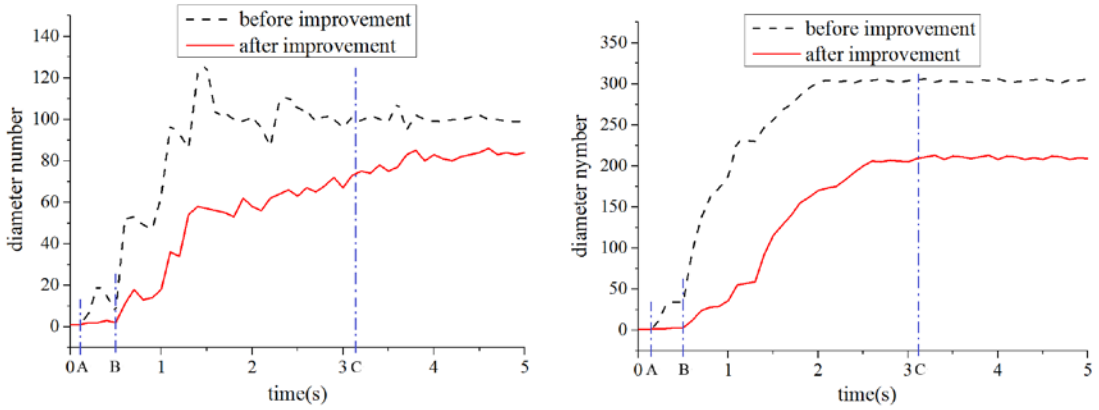

(a) Diameter number near coarse/fine interface (b) Diameter number in the whole area

Figure 11. Comparison of particle diameter number before and after improvement

Before the improvement, the diameter number of the particles start to rise when particles pass through the coarse/fine interface (time = A), so when the fluid hits the right wall and falls back (time = B), the diameter number of particles increases sharply. As the fluid continues to flow across the coarse/fine interface, the difference in diameter number is accumulated. When the simulation runs to C (time = C), the fluid flow tends to stabilize gradually, and the diameter number of particles has basically reached saturation. Up to the five seconds of the simulation, after the improvement, the number of particle diameter is reduced by 15% near coarse/fine interface, and in the whole calculation area, the number of particle diameter decreased by 32%. Although the particle interaction model we used in 2.2 can reduce the influence of the particle diameter difference on the calculation accuracy, after improvement, the robustness at coarse/fine interface is improved.

In order to verify the accuracy of the algorithm has been improved, we compared the experimental with simulation results of the position of water front in the dam-break problem as shown in Figure 12, after improvement, the simulation results are more consistent with the experiment compared with the previous algorithm. The algorithm accuracy of the scheme is improved by changing the decision method of particle entering the different resolution.

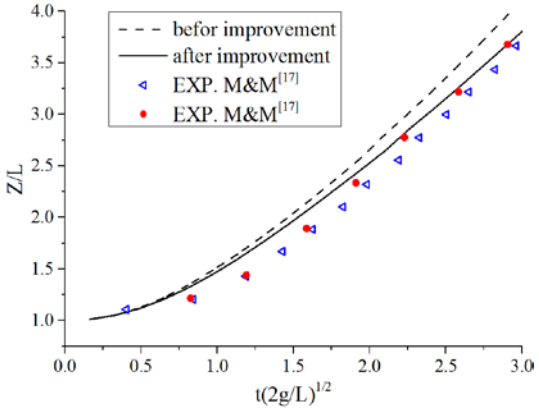

Figure 12. Experimental and simulation results of the position of water front in the dam-break problem

4.2 Moving High Resolution Region

In previous multi-resolution MPS methods, the high resolution region is fixed. In order to make the high resolution region move around the solid adaptively, we studied the influence of high resolution region movement on the flow field. We simulated the dam-break case as shown in Figure 5 with static high resolution region and moving high resolution region respectively. Figure 13 shows experimental and simulation results of the position of water

front in the dam-break problem, the simulation results obtained by the two methods almost coincide with each other, which proves that with moving high resolution region, the dynamic behavior of the fluid is not affected.

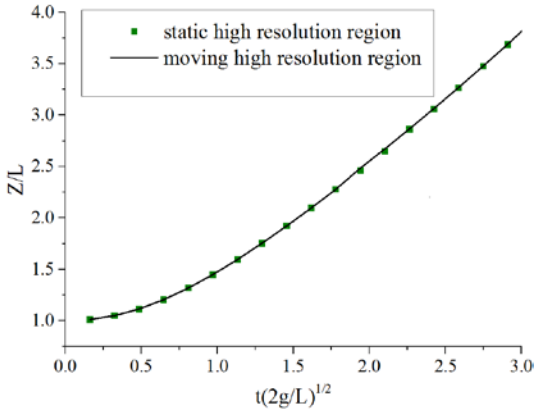

Figure 13. Experimental and simulation results of the position of water front in the dam-break problem

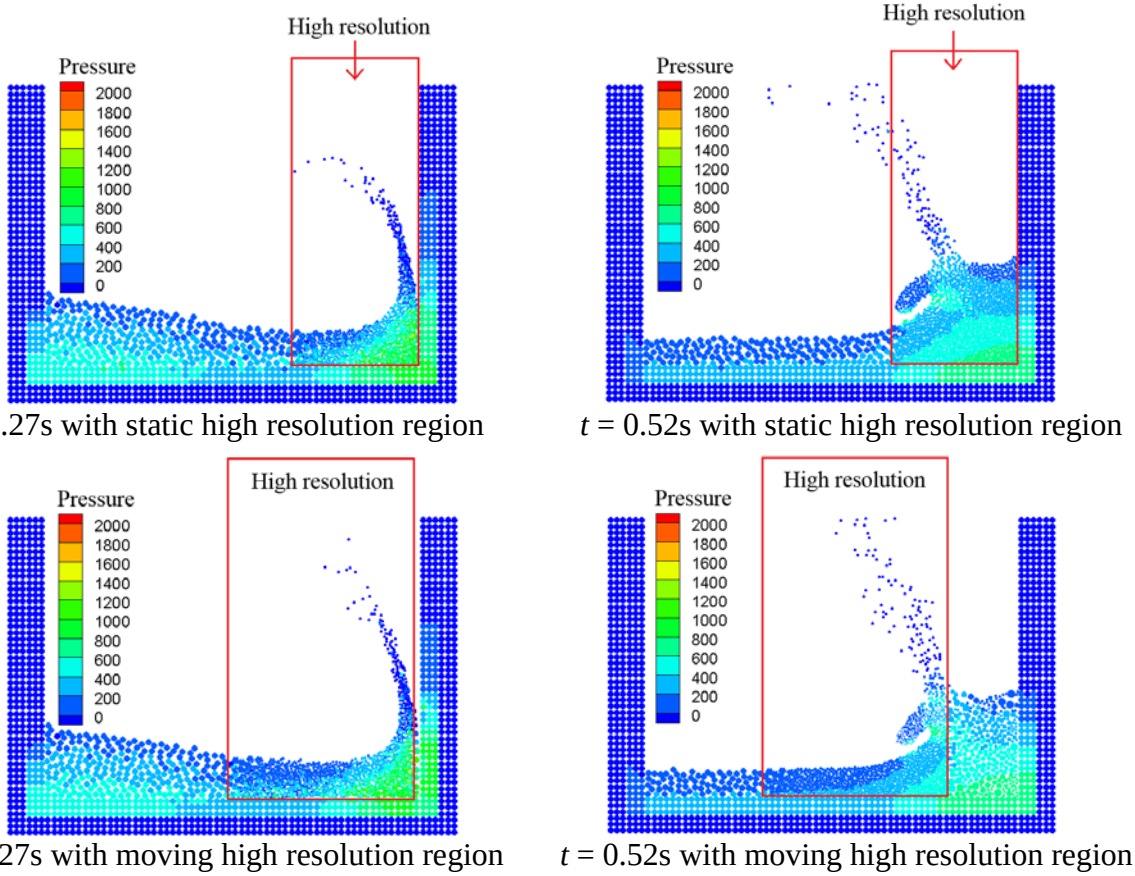

t = 0.27s with static high resolution region *t* = 0.52s with static high resolution region

t = 0.27s with moving high resolution region *t* = 0.52s with moving high resolution region

Figure 14. Snapshots from the dam-break simulation

Figure 14 shows the pressure distribution of fluid at two typical times with different methods, with moving high resolution region, the method can also accurately simulate the pressure distribution of fluid in the flow process.

In fact, as described earlier, the algorithm has realized that the splitting and coalescing processes can be conducted in the whole area, and the system can always keep the conservation of mass and momentum. The only difference between static resolution and moving resolution is the location of finer particles, so movable scheme can be very helpful if the location of the flow details we want to describe may change in the simulation. All the

above proves that the region movement has no adverse effect on the flow field, the scheme has been extended and the multi-resolution regions is fixed any more.

4.3 Adaptive Variable Size Particle MPS Model

In previous algorithm, the high resolution regions are static in space and known beforehand; all the particles that enter the high resolution regions are split into smaller particles. Since the high resolution region is static, it is not adaptive, in this paper, the scheme is improved with adaptive variable-size particle as AVSP-MPS, which means the shape and area of the domains with high resolution can be dynamically adjusted during the calculation according to the distance from a fluid particle to a movable object.

In this section, we use three methods, single resolution MPS, VSP-MPS and AVSP-MPS, to simulate the dam-break case with a moving obstacle, respectively. The schematic diagram is shown in Fig. 15. The density of fluid particles is ρ = 988kg/m^3, the viscosity is ν = 1.0 × 10^{6}m^2/s, the gravity is G = 9.8m/s^2, and the initial diameter of water particles is l_0 = 0.005m. The object moves in horizontal direction and the equation of motion can be expressed as **u** = -0.5×sin(2πt). The high resolution area in VSP-MPS simulation is static, so it is necessary to divide a large area into high resolution region (as shown in R_2 (red box) in Figure 15(a)). As a contrast, the high resolution region does not need to be given beforehand with AVSP-MPS method, the high resolution region can dynamically change in the simulation to ensure fine particles are always used around the moving obstacle (as shown in R_2 (red box) in Figure 15(b)).

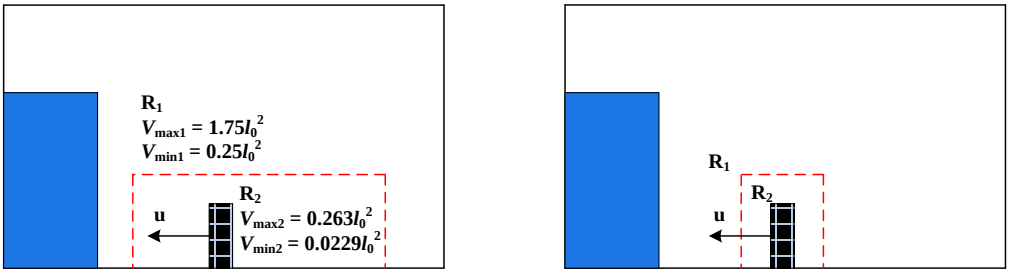

(a) VSP-MPS (b) AVSP-MPS

Figure 15. Geometry of the dam-break with obstacle

Fig. 16 shows the diameter distribution of fluid particles at several typical times using AVSP-MPS method, in the simulation, fine particles are only used around the moving obstacle, coarse particles are used in other area. It proves that the adaptive model has been successfully added to AVSP-MPS method, the high resolution area can dynamically change according to the distance between fluid particles to the moving obstacle.

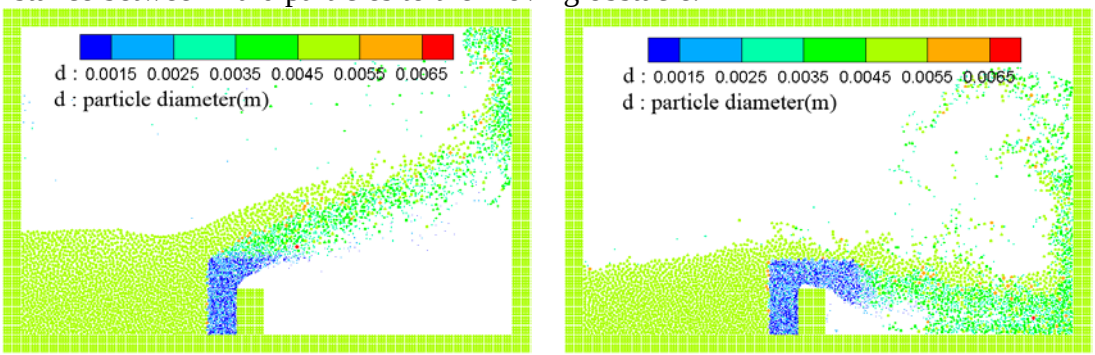

t = 0.4s *t* = 06s

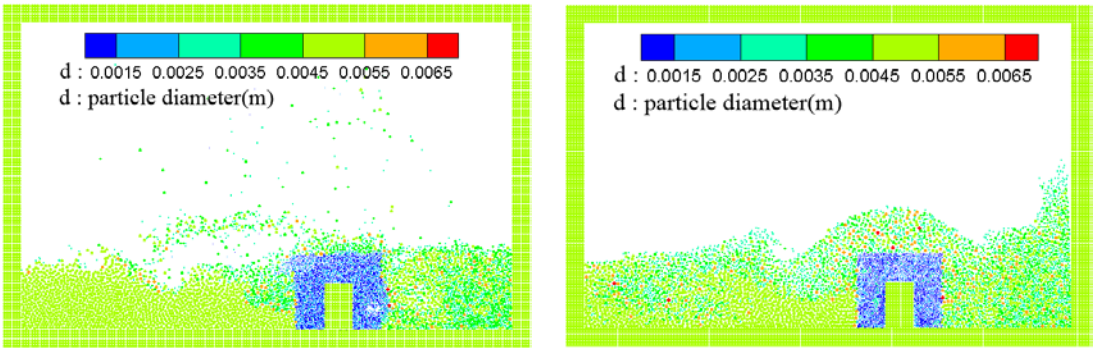

t = 1.0s t = 2.0s

Figure 16. Diameter distribution of the dam-break with obstacle

Fig. 17 shows the time-varying curves of particle number and CPU obtained by three methods. Compared with the single resolution MPS method, AVSP-MPS can greatly reduce the particle number and CPU time in the simulation process by 59.5% and 43.0%. Compared with the VSP-MPS method which can only delimit the resolution region in advance, AVSP-MPS method can reduce particle number by 49.5%, CPU time by 27.1%. With an adaptive algorithm, AVSP-MPS method can reduce the number of particles needed in the simulation and improve the calculation efficiency.

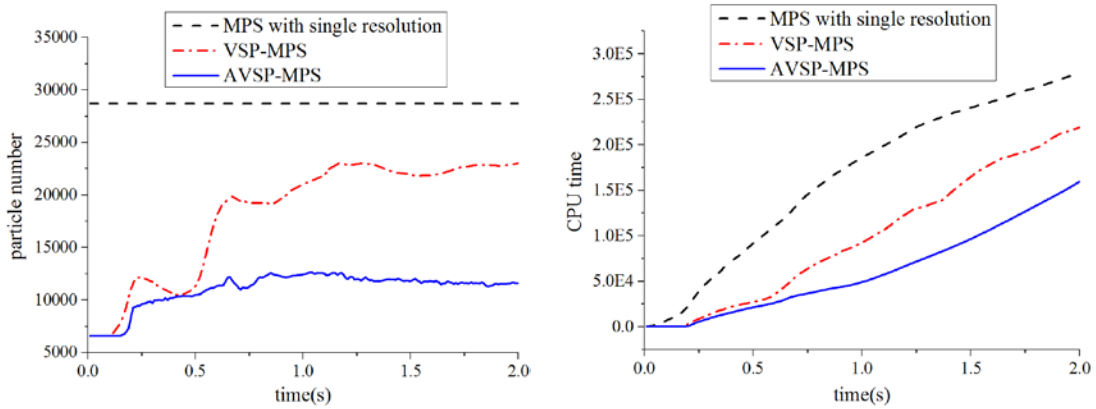

(a) Particle number (b) CPU time

Figure 17. Comparison of particle number and CPU time in different cases

5 Conclusions

In this paper, the scheme of MPS method is improved with adaptive variable-size particle as AVSP-MPS to increase computational efficiency. First, we made linear programming for the selection of resolution and got the optimal resolution interval, compared with MPS with single resolution, VSP-MPS method can reduce the number of particles needed for simulation and greatly shorten the calculation time. Then the algorithm is improved by changing the decision method of particle entering the different resolution to improve the robustness at coarse/fine interface. The improved approach is that only when the whole particle (the boundary of the particle) enters the high resolution region the particle splitting into finer particles. The algorithm accuracy of the scheme is improved by changing the decision method of particle entering the different resolution. As the high resolution of the previous multi-resolution MPS method is static, we get a moving high resolution region and studied the influence of high resolution region movement on the flow field, the region movement will not affect the flow field. At last, the scheme with adaptive variable-size particle as AVSP-MPS is introduced, the shape and area of the domains with high resolution can be dynamically adjusted during the calculation according to the distance from a fluid particle to a movable object. Compared with the VSP-MPS method which can only delimit the resolution region in

advance, with an adaptive algorithm, AVSP-MPS method can further reduce the number of particles needed in the simulation and improve the calculation efficiency.

References

[1] Koshizuka S, Oka Y. (1996) Moving-particle semi-implicit method for fragmentation of incompressible fluid. *Nuclear Science and Engineering* **123**:421–434.

[2] Liu, G. R. Liu, M. B. (2003) Smoothed particle hydrodynamics, a meshfree particle method, *World Scientific*, Singapore, 50–59.

[3] Omidvar, P., Stansby, P. K., Rogers, B. D. (2012) Wave body interaction in 2D using smoothed particle hydrodynamics (SPH) with variable particle mass, *International Journal for Numerical Methods in Fluids* **68**:686-705.

[4] Feldman, J., Bonet, J. (2007) Dynamic refinement and boundary contact forces in SPH with applications in fluid flow problems, *International Journal for Numerical Methods in Engineering* **72**:295-324.

[5] Vacondio, R., Rogers, B. D., Stansby, P. K. (2013) Variable resolution for SPH: A dynamic particle coalescing and splitting scheme, *Computer Methods in Applied Mechanics and Engineering* **256**:132-148.

[6] Chiron, L., Oger, G., Leffe, M. D., Touzé, D. L. (2018) Analysis and improvements of Adaptive Particle Refinement (APR) through CPU time, accuracy and robustness considerations, *Journal of Computational Physics* **354**:552-575.

[7] Sun, P. N., Colagrossi, A., Zhang A. M. (2018) Numerical simulation of the self-propulsive motion of a fishlike swimming foil using the δ^{+}-SPH model, *Theoretical & Applied Mechanics Letters* **8**, 115-125.

[8] Sun, P. N., Colagrossi, A., Marrone, S., Zhang A. M. (2017) The δplus-SPH model: Simple procedures for a further improvement of the SPH scheme, *Computer Methods in Applied Mechanics and Engineering* **315**. 25–49.

[9] Shibata, K., Koshizuka, S., Tamai, T., Murozono, K. (2012) Overlapping particle technique and application to green water on deck. *International Conference on Violent Flows* pp:160-111.

[10] Shibata, K., Koshizuka, S., Matsunaga, T., Masaie, I. (2017) The overlapping particle technique for multi-resolution simulation of particle methods. *Computer Methods in Applied Mechanics and Engineering* **325**, 434-462.

[11] Tanaka, M., Masunaga, T., Nakagawa, Y. (2009) Multi-resolution MPS method. *Trans. Jpn. Soc. Comput. Eng. Sci.* (in Japanese).

[12] Tang, Z.Y., Wan, D.C., Chen, G., Xiao, Q. (2016) Numerical simulation of 3D violent free-surface flows by multi-resolution MPS method. *J. Ocean Eng. Mar. Energy* **2**, 355-364.

[13] Chen, X., Sun, Z. G., Liu, L. Xi, G. (2016) Improved MPS method with variable-size particles. *International Journal for Numerical Methods in Fluids* **80**, 358-374.

[14] Chen, X., Xi, G., Sun, Z. G. (2014) Improving stability of MPS method by a computational scheme based on conceptual particles. *Computer Methods in Applied Mechanics and Engineering* **278**, 254-271.

[15] Tanaka, M., Cardoso, R. Bahai, H. (2018) Multi-resolution MPS method. *Journal of Computational Physics* **359**, 106-136.

[16] Tanaka, M., Masunaga, T. (2010) Stabilization and smoothing of pressure in MPS method by quasi-compressibility. *Journal of Computational Physics* **229**, 4279-4290.

[17] Martin J. C., Moyce W. J. (1952) An experimental study of the collapse of fluid columns on a rigid horizontal plane. *Philosophical Transactions of the Royal Society of London Series A* **244**, 312-324.